Available online at www.sciencedirect.com

ScienceDirect

Advances in Space Research 65 (2020) 74–85

ADVANCES IN SPACE RESEARCH
(a COSPAR publication)

www.elsevier.com/locate/asr

Ionospheric responses to the 21 August 2017 great American solar eclipse – A multi-instrument study

G. Uma [a], P.S. Brahmanandam [a,*], V.K.D. Srinivasu [b], D.S.V.V.D. Prasad [b], V. Sai Gowtam [c], S. Tulasi Ram [c], Y.H Chu [d]

[a] *Dept. of Basic Science, Shri Vishnu Engineering College for Women, Bhimavaram 534 202, Andhra Pradesh, India*
[b] *Dept. of Physics, Andhra University, Visakhapatnam 530 003, Andhra Pradesh, India*
[c] *Indian Institute of Geo-magnetism, Colaba, Mumbai, India*
[d] *Institute of Space Science, National Central University, Chung-Li, Taiwan*

Received 13 March 2019; received in revised form 13 August 2019; accepted 5 September 2019
Available online 16 September 2019

Abstract

Herein, we report on the ionospheric responses to a total solar eclipse that occurred on 21 August 2017 over the US region. Ground-based GPS total electron content (TEC) data along with ground-based measurements (Millstone Hill Observatory (MHO) and digital ionosondes) and space-based measurements (COSMIC radio occultation (RO) technique) allowed us to identify eclipse-associated ionospheric responses. TEC data at ~20°, ~30°, and ~40°N latitudes from the west to east longitudes show not only considerable depression but also wave-like characteristics in TEC both in the path of totality and away from it, exclusively on the day of eclipse. Interestingly, the observed depressions are associated with lesser (higher) magnitudes at stations over which the solar obscuration percentage was meager (significant), a clear indication of bow-wave-like features. The MHO observes a 30% reduction in F_2-layer electron densities between 180 and 220 km on eclipse day. Ionosonde-scaled parameters over Boulder (40.4°N, 100°E) and Austin (30.4°N, 94.4°E) show a significant decrease in critical frequencies while an altitude elevation is seen in the virtual heights of the F-layer only during the eclipse day and that decreases are associated with wave-like signatures, which could be attributed to eclipse-generated waves. The estimated vertical electron density profile from the COSMIC RO-based technique shows a maximum depletion of 40%. Relatively intense and moderate depths of TEC depression, considerable reductions in the F_2-layer electron densities measured by the MHO and COSMIC RO-measured densities at the F_2-layer peak, and elevations in virtual heights and reduction in the critical frequencies measured by ionosondes during the eclipse day could be due to the eclipse-induced dynamical effects such as gravity waves (GWs) and their associated electro-dynamical effects (modification of ionospheric electric fields due to GWs).

Keywords: Solar eclipse; TEC; Millstone hill observatory; COSMIC radio occultation technique; Ionosondes; Gravity waves

1. Introduction

Observations of eclipses (both solar and lunar) have been creating interest among both the public and space scientists since ancient times. The ancient Chinese and Babylon had recorded the spectacular events of eclipse way back in 2500 BCE, as they believed that planting and harvesting of crops, humans' health, and successes of significant persons were related to lunar and solar calendars (Gerasopoulos et al., 2008). On the other hand, eclipse observations provide an unprecedented opportunity for space scientists in probing the Earth's atmosphere to understand fundamental physical processes that connect the Sun, Moon, and the geospace system (Earth's neutral atmosphere and ionosphere).

* Corresponding author.
E-mail address: dranandpotula@svecw.edu.in (P.S. Brahmanandam).

https://doi.org/10.1016/j.asr.2019.09.010
0273-1177/

The Earth's ionosphere is affected by several disturbances including solar flares, coronal mass ejections (CMEs), geomagnetic storms, and solar eclipses. Among these disturbances, ionospheric eclipse observations create a definite contribution to study transient properties, which can be attributed to the sudden decreases in ionizing radiation from the Sun during solar epochs. Although earlier researchers reported that the Earth's atmosphere responds to changes in solar illumination (Mitra, 1952 and references therein), Chimonas (1970) and Chimonas and Hines (1970) were the first researchers to report that a sudden cooling effect would act as a potential source of gravity waves (GWs) that are capable to propagate up to even thermospheric altitudes, when the source mechanism propagates with supersonic speeds. The created GWs, eventually, build up as bow-waves (Liu et al., 2011). Liu et al. (2011), in their research, had provided evidence on ionospheric bow-waves during the 22 July 2009 solar eclipse by effectively applying an advanced analysis technique, i.e., Hilbert Huang Transform (HHT, Huang et al., 1998), on ionospheric TEC derived from ground-based GPS receivers in Taiwan and Japan.

Fortunately, for the first time in 26 years, a complete (total) solar eclipse occurred over the continental United States (CONUS) on 21 August 2017, wherein a dense set of ground-based ionospheric sensors were installed and ~4000 GPS receivers with millions of *trans*-ionospheric lines of sight were available (Zhang et al., 2017; Cherniak and Zekharenkova, 2018). This relatively dense coverage, continuous, and unprecedented resolutions of GPS-based observations would be an advantage when unique observational results are sought. As such, several research studies have reported excellent results, for the first time, by virtue of the availability of GPS-based observations. For example, Huba and Drob (2017) reported the first simulation prediction of the 21 August 2017 solar eclipse-associated impact on the ionosphere/plasmasphere system using the $SAMI_3$ model. Later, Coster et al. (2017) critically analyzed GPS-based data to study the latitudinal and longitudinal variations of TEC and the presence of traveling ionospheric disturbances (TIDs) during the 21 August 2017 solar eclipse. With an intention to detect the 21 August 2017 solar eclipse-generated GWs (Chimonas and Hines, 1970), GPS-derived TEC data along and across the eclipse path have been analyzed by Nayak and Yigit (2017), and they observed GWs with wave periods of approximately ~20–90 min at all locations both in the path of totality and away from it. Crystal clear ionospheric disturbances as ionospheric bow-waves (which are similar to a fast-moving riverboat) were detected by analyzing differential TEC data during the 21 August 2017 solar eclipse (Zhang et al. 2017, see their Figs. 1 and 2). It may not be an exaggeration that the 21 August 2017 eclipse event had provided a unique opportunity for researchers worldwide to identify eclipse-associated ionospheric disturbances in the form of TIDs unambiguously, which could be due to the availability of several ground-based GPS receivers.

This research considers multi-instrument databases generated out of various remote sensing instruments including the Millstone Hill Incoherent Scatter Radar (ISR), COSMIC RO technique, Digisonde ionosonde radars, and GPS TEC data to study ionospheric responses to the 21 August 2017 solar eclipse. The ensemble of a good number of remote sensing instruments has allowed us to verify ionospheric responses to the 21 August 2017 solar eclipse unambiguously and, as an effect, important research results are found. This research paper is organized as follows: Section 2 discusses about the various databases that we used in

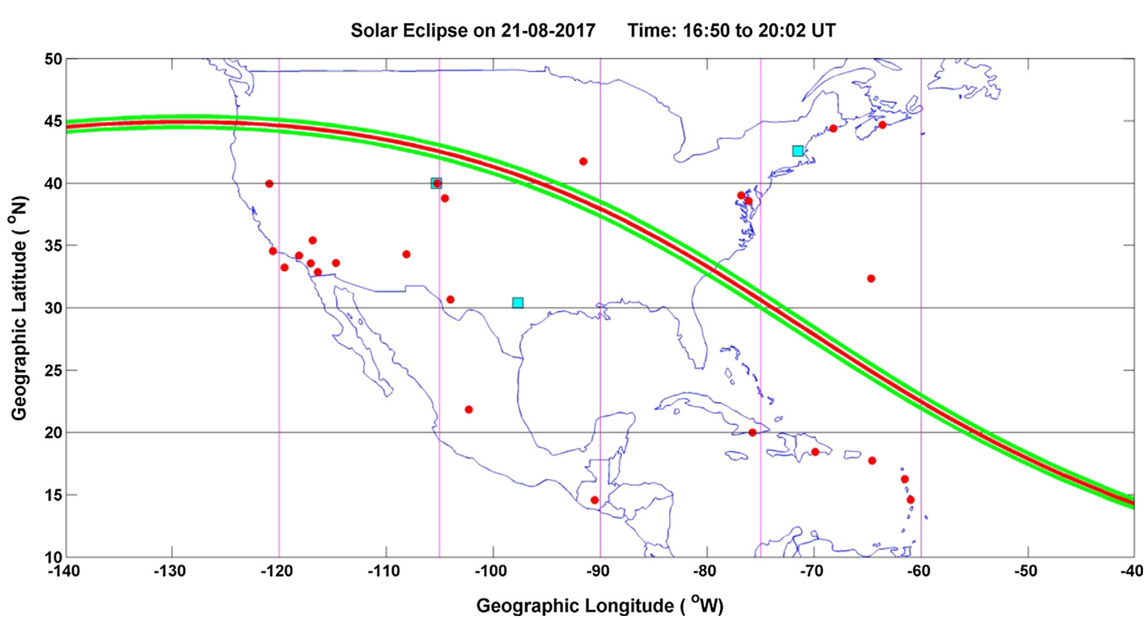

Fig. 1. Locations of the IGS stations (red circles), DIDBASE ionosonde stations (magenta squares), and path of the solar eclipse (green – partial, red – totality, and green – partial). (For interpretation of the references to color in this figure legend, the reader is referred to the web version of this article.)

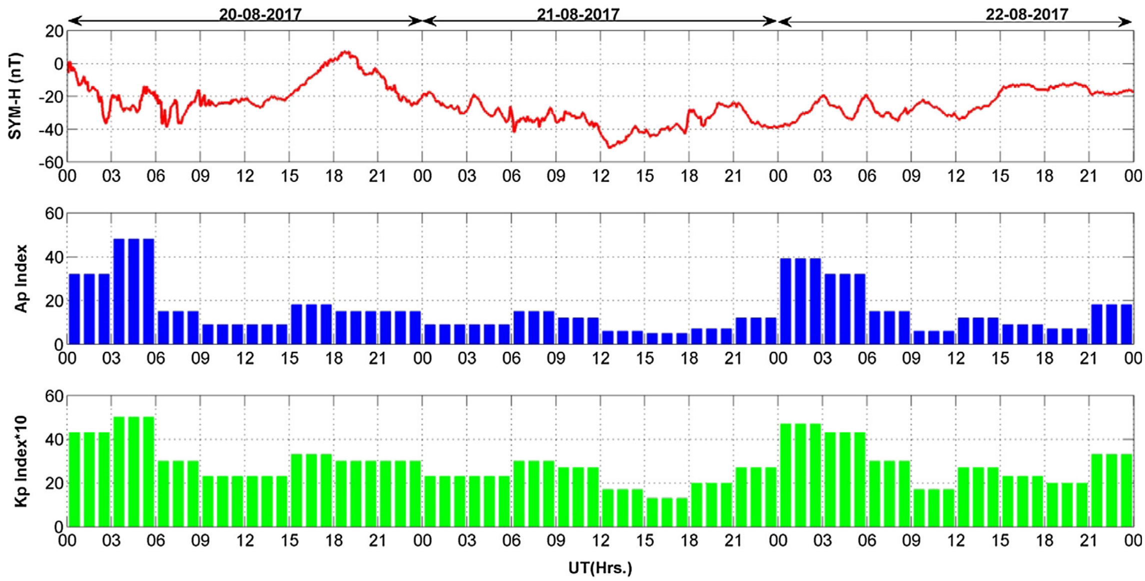

Fig. 2. Geomagnetic conditions during 20–22 Aug 2017 including SYM-H, Ap index, and Kp index.

this study and the adopted methodology. In Section 3, we present various observational results of various remote sensing instruments including MHO, digital ionosondes, COSMIC RO, and TEC measured using ground-based GPS receivers. The discussion part is presented in Section 4, followed by the conclusion in Section 5.

2. Database and methodology

Electron density profiles (Ne(h)) retrieved by the COSMIC RO satellites are critically evaluated to verify the 21 August 2017 solar eclipse effects on the ionosphere, for which all the satellite lines of sight around the time of eclipse totality have been considered. A constellation of six low earth orbiting (LEO) micro-satellites, named as COSMIC (Constellation Observing System for Meteorology, Ionosphere, and Climate), were deployed at 512 km on 15 April 2006; they later dispersed to an 800 km altitude (Cheng et al., 2006) to receive radio signals from Global Positioning System (GPS) using the RO technique (Kursinski et al., 1997). The COSMIC RO, a space-based method, has been proved to be one of the effective and accurate methods in providing lower (Brahmanandam et al., 2010; Anthes, 2011) and ionospheric (Potula et al., 2011; Brahmanandam et al., 2011; Brahmanandam et al., 2012; Uma et al., 2016; Uma et al., 2019) data products including temperature, water vapor, relative humidity, and ionospheric electron density with unprecedented resolutions. In this study, we used post-processed Ne(h) (data product name – “ionPrf”) that were collected from the CDAAC (COSMIC Data Analysis and Archive Center) website, www.cdaac.cosmic.ucar.edu. Electron density profiles, Ne(h) probed by the Millstone Hill ISR, which operates with a zenith-directed 68 m fixed parabolic antenna and a fully steerable 46 m antenna (Holt et al., 2002), are considered in this study. The Millstone Hill ISR data were archived from the Madrigal online database system (http://www.openmadrigal.org) hosted by MHO. To study the changes caused by the solar eclipse in the E- and F-regions near to the eclipse path, ionospheric parameters recorded by two Digisonde ionospheric sounders are utilized, which are located at Boulder (40.0° N, 105.3° W) and Austin (30.4° N, 97.7° W). Further, GPS receivers-measured ionospheric TEC is used to monitor the ionospheric variations induced by the solar eclipse. It was reported by Zhang et al. (2017) that more than 2000 GPS receivers were deployed over the CONUS to monitor TEC variations induced by the 2017 solar eclipse. Fig. 1 shows the path (including central, north, and south) of the 21 August 2017 solar eclipse and various ground-based instruments used in the present study (see figure for more clarity). The magnetic activity level, as shown in Fig. 2, on 21 August 2017 was rather quiet, with K_p values lying below 3 during most of the time. Fig. 1 also shows the respective SYM-H and Ap-index values.

3. Results

3.1. COSMIC RO-based measurements

Fig. 3a shows two COSMIC RO-retrieved typical electron density profiles (Ne(h)) at approximately 2100 UT during the eclipse day, i.e., 21 August 2017 (a thick blue line and its smoothed curve is shown as a thick red line) as well as during the non-eclipse day, i.e., 20 August 2017, which is considered as background Ne(h) (a thick black line), and Fig. 3b shows the percentage reduction in electron density. Note that the COSMIC satellites’ horizontal projections (black and blue inclined lines), the eclipse path (northern, central, and southern limits included), and the geographical location of the MHO (a red dot) are shown in the inset figure (see, Fig. 3a). It has

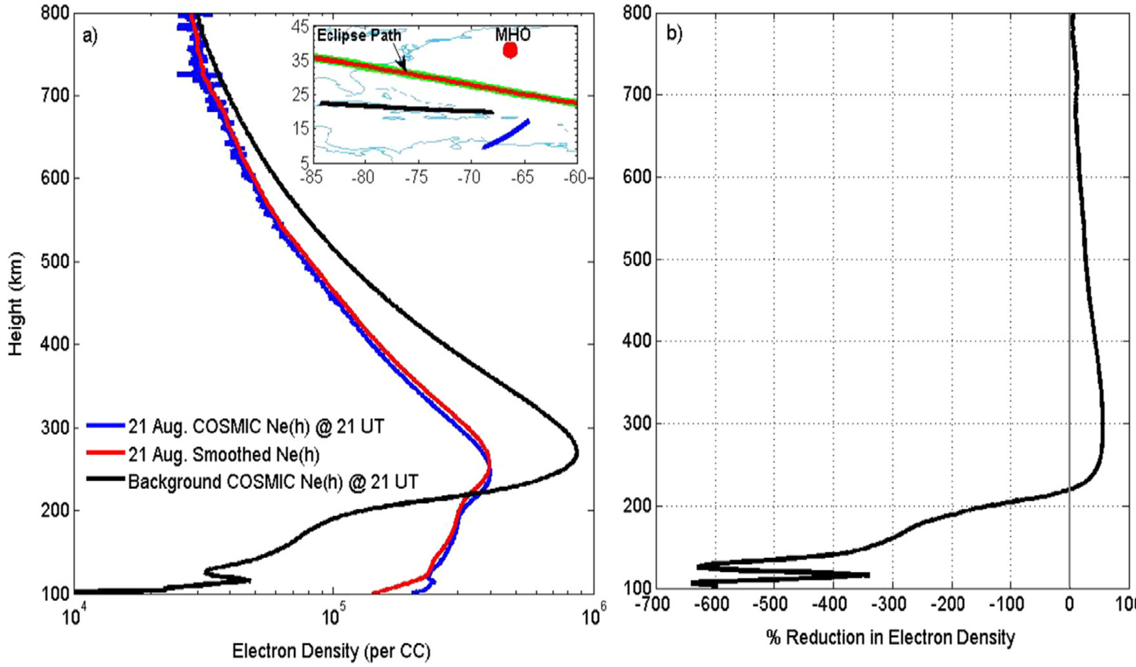

Fig. 3. (a) Variation in electron density profiles (Ne(h)) retrieved by the COSMIC RO satellites over the US region for the eclipse day (21 August 2017) and back ground Ne(h) during a non-eclipse day (20 August 2017). The smoothed electron density profile on the eclipse day is also shown, and (b) the percentage reduction in electron density as compared to the smoothed electron density profile is presented. The COSMIC satellites' horizontal projections (black and blue continuous lines) are shown in the inset Fig (see the topside right space in panel "a") during 20 and 21 August 2017 along with the path of solar eclipse and the geographical location of Millstone Hill Observatory (MHO). (For interpretation of the references to color in this figure legend, the reader is referred to the web version of this article.)

been well documented that the retrieval errors of the electron densities using GPS RO techniques at the bottom of the ionosphere at mid and low latitudes may be as large as 100% or more, while those in the main F region around peak height and above are in general less than 10–20% (e.g., Chu et al., 2009; Wu et al., 2015). Therefore, the extraordinarily high electron densities below approximately 200 km presented in Fig. 3a were very likely dominated by the COSMIC RO retrieval errors and became unreliable. Fig. 3b shows the reduction in electron density that started from ~220 km onwards and continued up to 800 km altitude range, but a maximum reduction (more than 40%) is observed near to the F-region altitudes, i.e., between 240 km and 420 km with a peak (~57%) at 297 km. This maximum reduction indicates that the concentration of particles is affected heavily by the obscurity, which is in the crucial region of the ionosphere, i.e., the ionospheric F-region, and the peak corresponds to approximately 350 km altitude (Rishbeth and Garriott, 1969).

3.2. Millstone hill observatory (MHO) incoherent scatter radar (ISR) measurements

Ionosphere response over MHO (42. 61° N, 71. 49° W), Westford (a mid-latitude station in the USA), to the 21 August 2017 solar eclipse is also presented in the following lines, and the present eclipse track caused the MHO site to experience a near-70% magnitude partial eclipse (Zhang et al., 2017). Fig. 4 presents electron densities (N_e), wherein the top, middle, and bottom panels show N_e during 21 August (the eclipse day) and 22 August (a control day) along with deviations of Ne between 21 August and 22 August 2019. Note that the start, peak, and end timings of eclipse obscuration over MHO are marked onto the plot with dotted, continuous, and dotted lines, respectively, and these timings are found to be 1724 UT, 1842 UT, and 1954 UT, respectively. A striking feature noted from these figures is that a valley-like deep reduction is found in electron densities (approximately 30%) between the 180 km and 220 km altitude range between 1800 and 1930 UT on 21 August, while no such valleys were found on 22 August. Further, a keen observation of the top panel of Fig. 4 reveals that a moderate reduction (~20%) in N_e appeared above ~280 km that started from approximately 1100 UT onwards (before the eclipse start time) and continued until approximately 2030 UT. Interestingly, the lower F-region (ionosphere between 180 and 220 km altitude range) recovered from the reduction in Ne by 1930 UT, whereas it took approximately one hour additionally for the upper F region to recover from the reduction. The slow response of the upper F region as compared to that in the lower F region to the solar eclipse events could be attributed to the longer recombination times of electrons, and further, the eclipse-induced effects would be controlled by the transport of the plasma. With regard to the deviations of electron density profile (Ne(h)), as shown in the bottom panel of Fig. 4, it is very clear that a strong depletion in electron densities occurs between 200 km and 280 km,

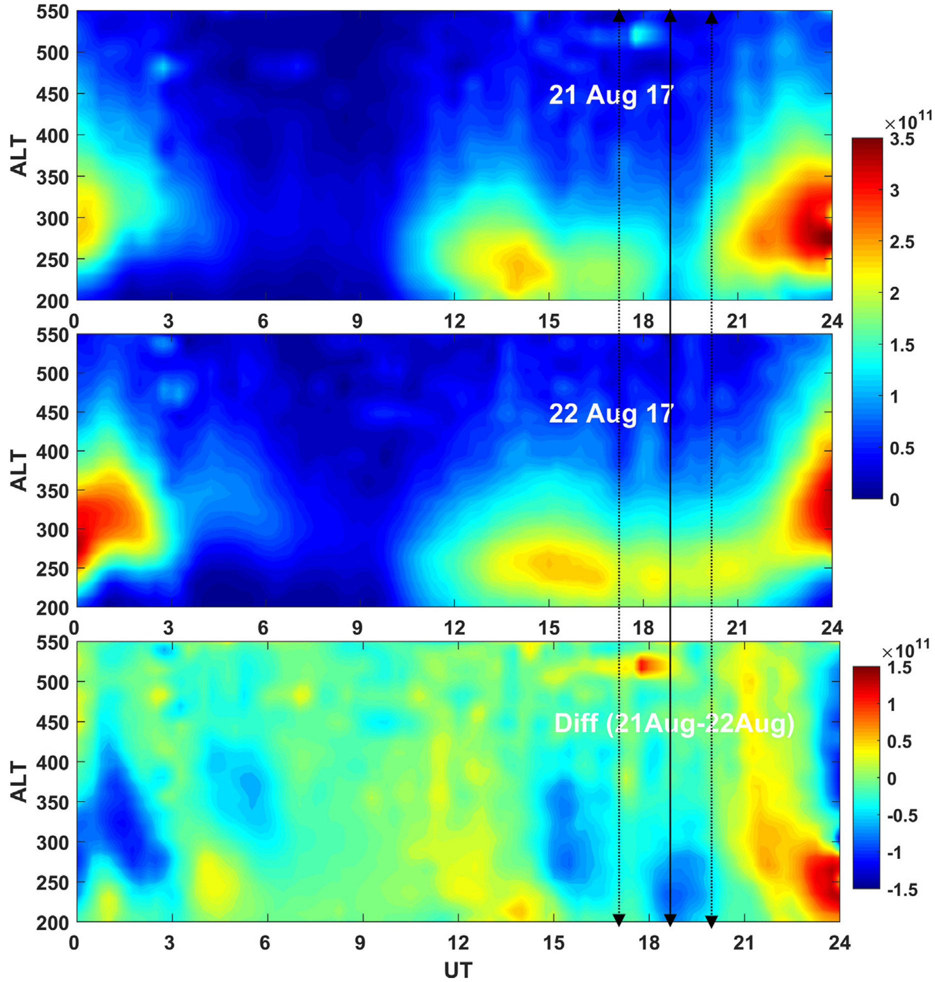

Fig. 4. Temporal vs. altitudinal variations in electron density (in logarithmic scale) profiles probed by the Millstone Hill ISR during 21 August (top panel) and 22 August 2017 (middle panel) and also shown deviations of electron densities (21–22 Aug. 2019) in the bottom panel. The start, maximum, and end times of the eclipse are shown with dotted, continuous, and dotted lines in the figures.

and the maximum depletion at approximately 240 km is seen approximately between 1840 and 1845 UT during which the maximum eclipse obscuration occurred over Millstone Hill radar. This strong depletion in Ne(h) could be due to the eclipse-associated effects (Evans, 1965a, 1965b; Salah et al., 1986; Pitout et al., 2008). For instance, Evans (1965a, 1965b) reported the responses of various ionospheric parameters including electron density (N_e), electron temperature (T_e), and ion temperature (T_i) over the Millstone Hill Observatory for the 23 July 1963 solar eclipse, and it was observed that although a considerable decrease in T_e and T_i occurred, T_e show a sudden drop. Another eclipse occurred over this station on 30 May 1984 during which a 60% reduction in electron density was found between the 130 and 250 km altitude range (Salah et al., 1986). Recently, Pitout et al. (2008) observed depletion in electron density (10%) in the lower F region of the ionosphere over Svalbard (78.2°N, 15.5° E) ISR site, Norway in response to the 1 August 2008 solar eclipse.

3.3. Digital ionosonde measurements over Boulder and Austin

Concerning the effects of the solar eclipse on the E- and F-regions, ionospheric parameters including f_{min} (lowest frequency at which an o-mode echo is observed on the ionogram), f_oE (critical frequency of the E-layer), f_oF_2 (critical frequency of the F2-layer), and h'E (virtual height of the E-layer), h'F (base height of the F-region), and h'F_2 (virtual height of the F_2-layer) are chosen. Figs. 5 and 6 show the diurnal variations (both in universal time (UT) and local time (LT)) of various ionospheric parameters over Boulder (40.0° N, 105.3° W) and Austin (30.7° N, 97.7° W), wherein the start, peak, and end timings of the solar eclipse are marked with dotted and continuous lines. Also shown are the 15 quite day averages during pre (post) eclipse epoch in blue (green) along with the eclipse day values (red). Note that the ionospheric parameters presented in this study were manually scaled so carefully from individual ionograms and their time resolution was 15 min. In general, a relatively

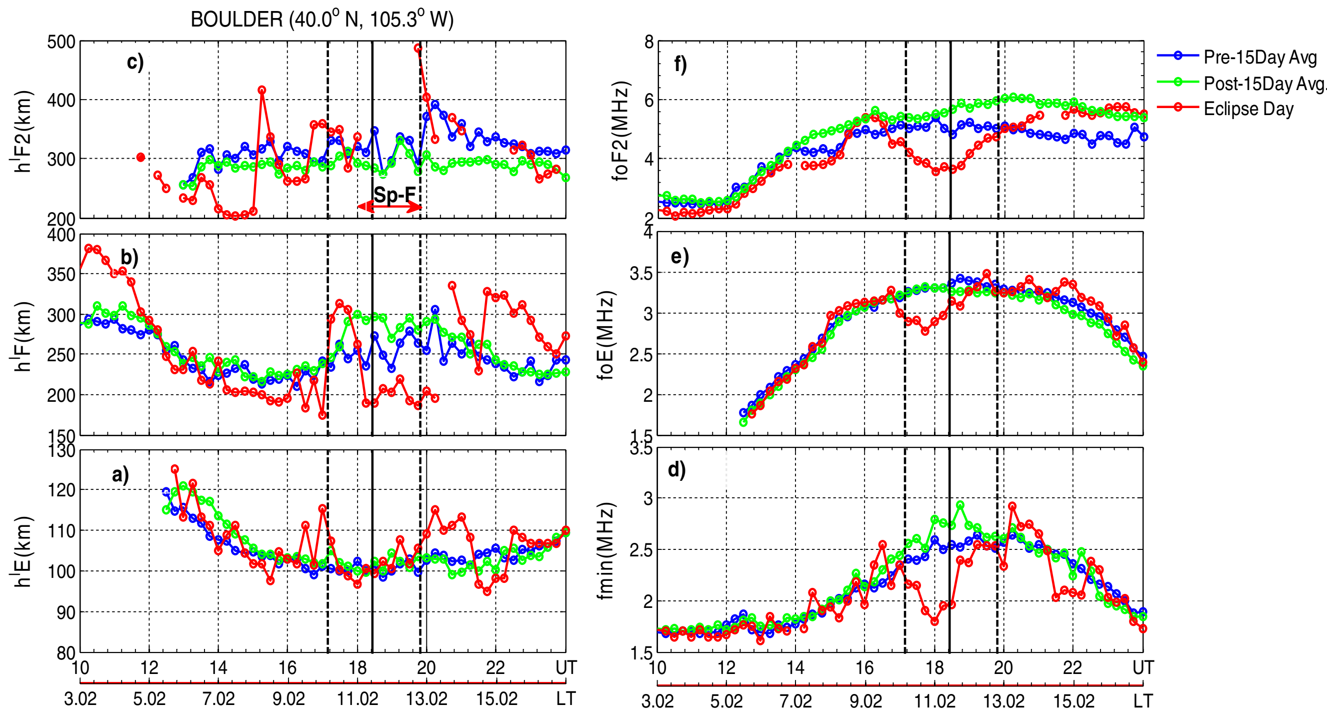

Fig. 5. Diurnal variations in ionosphere parameters including h'E, h'F, and h'F_2 in km and fmin, f_oE, and f_oF_2 in MHz over Boulder (40.0° N, 105.3° W), in which a fifteen-day average (blue line) before the eclipse day and post-eclipse (green line) is also shown along with eclipse day (red line) values. (For interpretation of the references to color in this figure legend, the reader is referred to the web version of this article.)

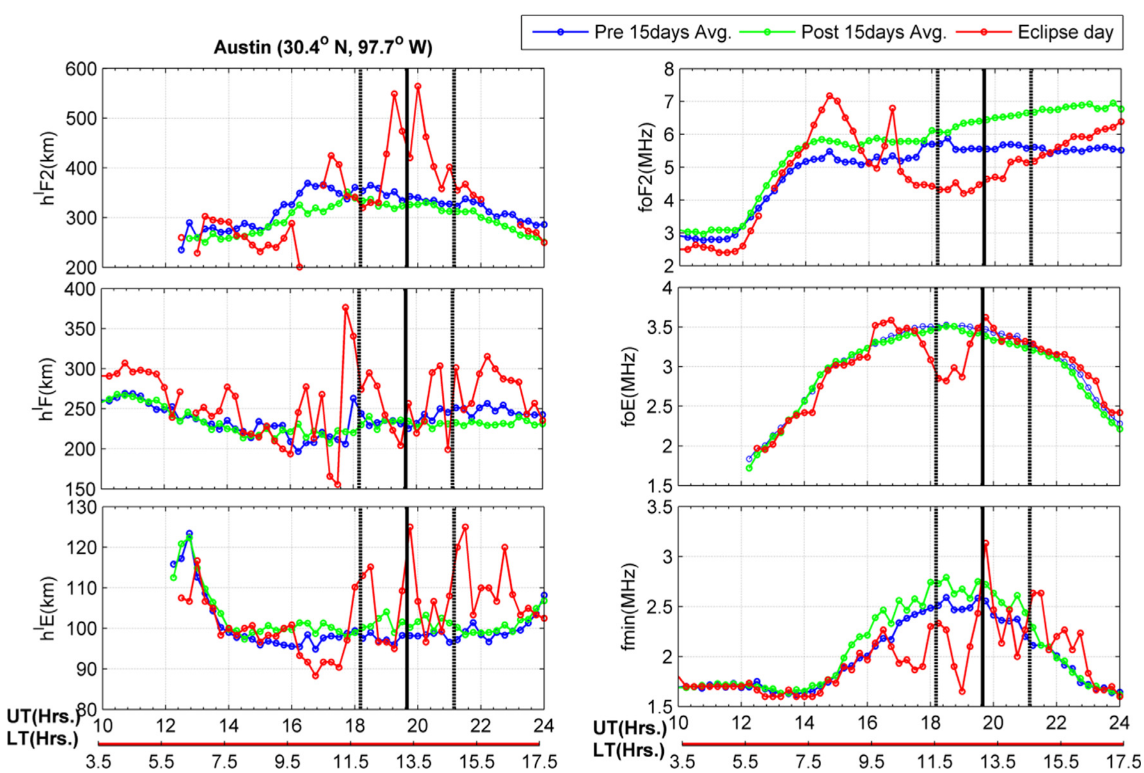

Fig. 6. Diurnal variations in ionosphere parameters including h'E, h'F, and h'F_2 in km and fmin, f_oE, and f_oF_2 in MHz over Austin (34. 4° N, 97.7° W), in which a fifteen-day average (blue line) before the eclipse day and post-eclipse (green line) is also shown along with eclipse day (red line) values. (For interpretation of the references to color in this figure legend, the reader is referred to the web version of this article.)

high sampling time would be preferred for events like solar eclipse (Verhulst et al., 2016). In this context, the usage of the relatively lower sampling rate of ionograms may not reveal finer structures of wave-like signatures observed in various ionospheric parameters, particularly of traveling ionospheric disturbances (TIDs). Nevertheless, as the characteristic features of TIDs vary between 10 and 30 min (Stankov et al., 2017), the present study is still capable of unraveling TID signatures.

It is obvious from the bottom panel of Fig. 5 that no significant deviations in pre- and post-eclipse day values are noticed in h'E (the virtual height of the ionospheric E-layer), but h'E values during the solar eclipse day show a sudden increase in the beginning of the solar eclipse, i.e., from 1620 UT onwards, and there was a sudden decrease in h'E values during solar eclipse epoch, followed by an increase in h'E once again. This regular increasing, decreasing, and increasing trends of h'E might be possibly due to GWs produced at the lower altitudes due to the present solar eclipse. Further, the quick response of h'E values, particularly on solar eclipse day, is a quite interesting and understandable aspect. As the lower ionosphere (~below 180 km) reacts immediately to the solar disc obscuration (Jakowski et al., 2008), it may conclude here that the wave-like nature of h'E can be attributed to the solar eclipse-induced effects. On the other hand, it is quite clear from the middle panel of Fig. 5 that h'F on the eclipse day increased to higher values by ~50 km immediately after the onset of eclipse (~1702 UT) and that trend continued for approximately 30 min. Beyond that, there was a sudden drop in eclipse day values, and later, these values were somewhat comparable with average values. The h'F2 values, as can be seen in Fig. 5c, showed higher magnitudes starting from just past eclipse peak timings (1800 UT) and seemed to reach a higher altitude (~500 km) by 1948 UT. As expected, the higher altitude zone between 1800 UT and 1948 UT had been associated with strong spread-F (Sp-F) activity, which is marked as a double-arrow symbol in the figure (red color arrow). A time delay exists between the responses of h'F and h'F_2 to this solar eclipse, which can be attributed to different dynamics and photochemistry that exist at the respective altitudes. More clearly, the bottomside ionosphere is primarily controlled by the local solar radiation, while the ionosphere at peak altitudes (h'F_2) and further above (topside ionosphere) is rather influenced by processes of the plasma redistribution (Cheng et al., 1992). On the other hand, a definite reduction in plasma frequencies on the eclipse day is seen that is presented on the right side of Fig. 5. More clearly, a moderate decrease in the critical frequencies of E- and F_2-layers and fmin was started without any delay (between the time of maximum obscuration and the time of maximum reduction), and these decreases were found to be approximately 30%, 40%, and 21%, respectively. As the amount of solar radiation incident on the ionosphere decreases, the ionospheric ionization also decreases, which causes a decrease in electron density, and hence, foF_2 decreases. The measured peak plasma frequencies in the F_2 layer (foF_2) were near 4.0 +/− 0.5 MHz, with the height of F_2 layer peak, hmF_2, ranging between 196 km and 244 km. According to the INAG (Ionosonde Network Advisory Group) newsletter on the 2017 solar eclipse effect, the maximum plasma frequency of the F_2 layer (foF_2) was reduced up to 30%, and its corresponding height, hmF_2, dropped by ~100 km.

The diurnal variations (both in UT and in LT) of various ionospheric parameters over Austin (30.7° N, 97.7° W) as shown in Fig. 6 are showing few differences as compared to the scenario over Boulder. Importantly, a wave-like nature persistently appeared in h'E before the start time and continued beyond the end time of the eclipse. It is worth mentioning here that Boulder (Austin) experienced a 93% (65.2%) solar obstruction during the peak of the eclipse, which means the overlying ionosphere over Boulder had responded more quickly than that over Austin. Further, a similar wave-like behavior appeared in h'F and h'F_2 during the start, peak, and end times of the eclipse, and these wave-like oscillations maintained very near similitude with the oscillations that occurred in the ionospheric E-layer. It is well known that the lower ionosphere (~below 180 km) reacts immediately to the solar disc obscuration, whereas the electron densities of the ionosphere above 180 km decrease with a delay of approximately 30 min (Jakowski et al., 2008). Nevertheless, no such delay has been seen in h'F and h'F_2, which is in contrast with the Jakowski et al. (2008) research results. On the other hand, a definite reduction in fmin, f_oE, and foF_2 is seen (see, right panel of Fig. 6), although a few differences could be seen in various places in foF_2. Moderate to lower decreases are observed in fmin and the critical frequencies of F_2-layer and E-layer, which are 40%, 33%, and 36%, respectively. These sudden and deep depressions could be most possibly due to the eclipse-associated effects.

A few important studies carried out in European countries with similar observational results have also appeared in the literature. For instance, a moderate increase (decrease) in plasma frequencies (virtual heights) is also observed over Belgium (50.1° N, 4.6° E) during a partial solar eclipse that occurred on 20 March 2015 (Verhulst et al., 2016). By properly utilizing high-resolution Digisonde radar apart from ionospheric tilt and drift measurements, Verhulst et al. (2016) surmised that a bow-wave-like disturbance generated in the neutral atmosphere due to the shadow of the moon and that bow-wave could be a possible source of wave-like characteristics in the overlying ionosphere. Similarly, a high-quality multi-instrument study carried out in Belgium and European regions to understand the response of the overlying ionosphere to the 20 March 2015 solar eclipse by Stankov et al. (2017) revealed that TID signatures were found in electron density depletions with periodicities of approximately 10–15 min.

3.4. GPS-based TEC measurements

The diurnal variations of TEC, presented in TEC units (one TECU = 10^{16} el/m^2), in longitude sectors spanning from ~120° W to ~60° W at various latitudes allowed us to evaluate the ionospheric response to the solar eclipse. Figs. 7a–7c show the diurnal variations of TEC at ~20°, ~30°, and ~40° latitudes, in which blue, green, and red lines represent TEC variations during pre-eclipse (20 August), post-eclipse (22 August), and the eclipse day (21 August), respectively. The open circle on each station TEC data denotes the time of the maximum eclipse for that location, and the percentage of obscuration of the eclipse over the particular station on individual plots is shown.

To verify whether wave-like signatures present or not in TEC triggered by the eclipse-associated effects, we plotted the diurnal variations of TEC at different sectors from the west to east longitudes at various latitudes. The important observations from these stacked-diagrams shown in Figs. 7a–7c are as follows: (i) The diurnal variations of TEC during the eclipse day showed a continuous decrease from ~1600 UT onwards, and this decrease intensified by approximately 1700 UT to reach as minimum as approximately 6–8 TECU at the majority of the stations. (ii) TEC variations during pre- and post-eclipse days had shown ~10–12 TECU, which quantitatively shows that the TEC values during the eclipse day (21 August) were only approximately ~40–45% of pre- and post-eclipse day values. (iii) The recovery of TEC values on the eclipse day started by approximately 2200 UT. And (iv) Most importantly, a deep valley in TEC has a wave-like nature during the eclipse day moving steadily almost with the progress of time from the west to east longitudes, and the amplitude of such valley is found to have increased at stations with a maximum obscuration percentage and shows decreasing trends at stations with minimum obscuration percentage. It may be understood from these valley observations that the magnitude and wave-like nature decrease irrespective of whether the station is located above or below the station with maximum obscuration, which is clear evidence of the presence of a bow-wave in TEC. As expected, no such features are observed during 20 (pre-eclipse) and 22 (post-eclipse) August 2017, which implies that the overlying ionosphere on the eclipse day (21 August) was affected by the eclipse.

4. Discussion

Regular ionospheric effects of solar eclipses are fairly well understood since a long time (for example, see Evans, 1965a, 1965b; Brahmanandam et al., 2013). Further, eclipse-associated ionospheric effects in terms of changes in electron density in various layers of the ionosphere over the low- and mid-latitudes have been well characterized (Jakowski et al, 2008, and references therein). Indeed, concrete experimental evidence on the generation of GWs and their consequent effects on the overlying ionosphere is not yet fully explored over the larger area, primarily due to the lack of a dense and high sampled database. Nevertheless, the present eclipse has provided an excellent opportunity for researchers to observe the generation of GWs over a large area (see the research findings of

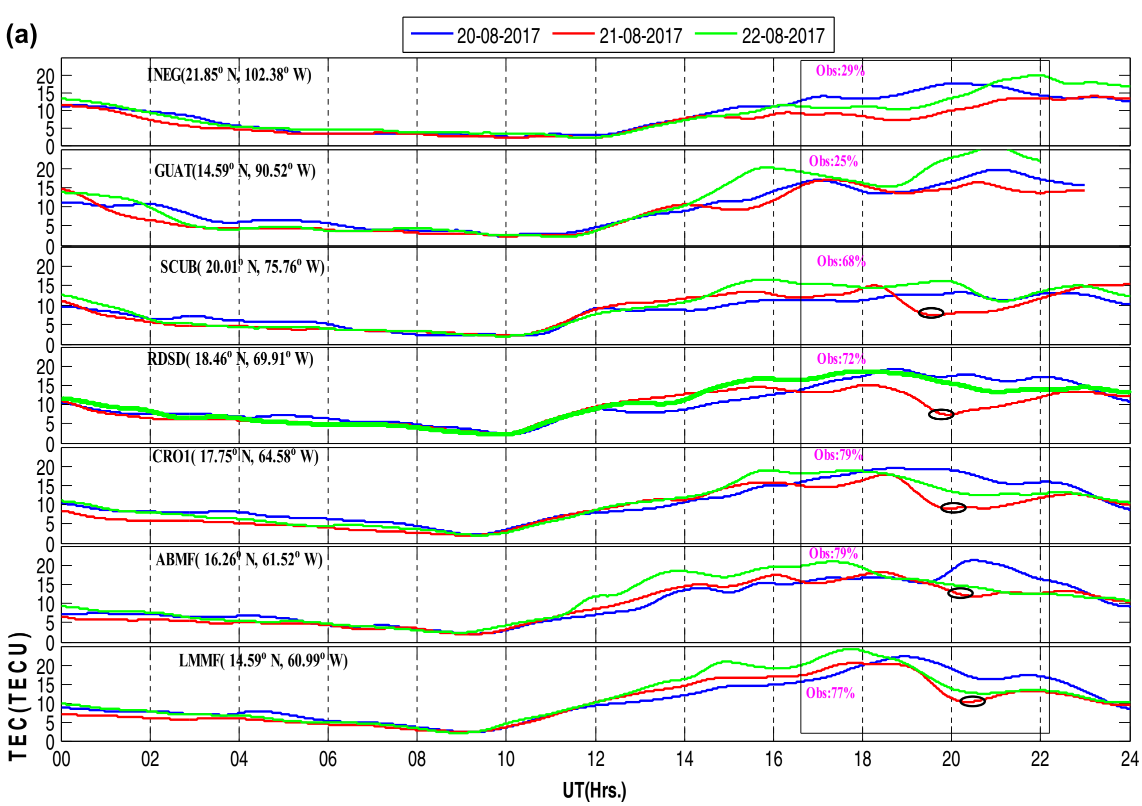

Fig. 7a. GPS measurements in TECU at ~20° on 21 August 2017.

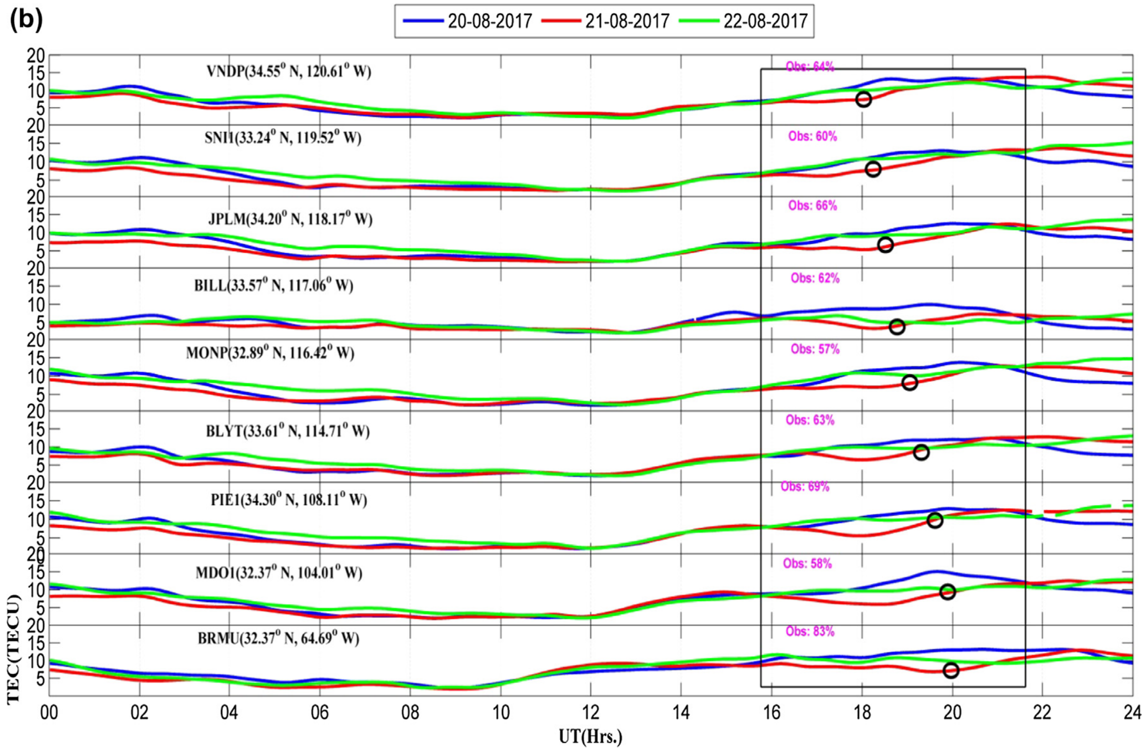

Fig. 7b. The same as Fig. 7a but at ~30° on 21 August 2017.

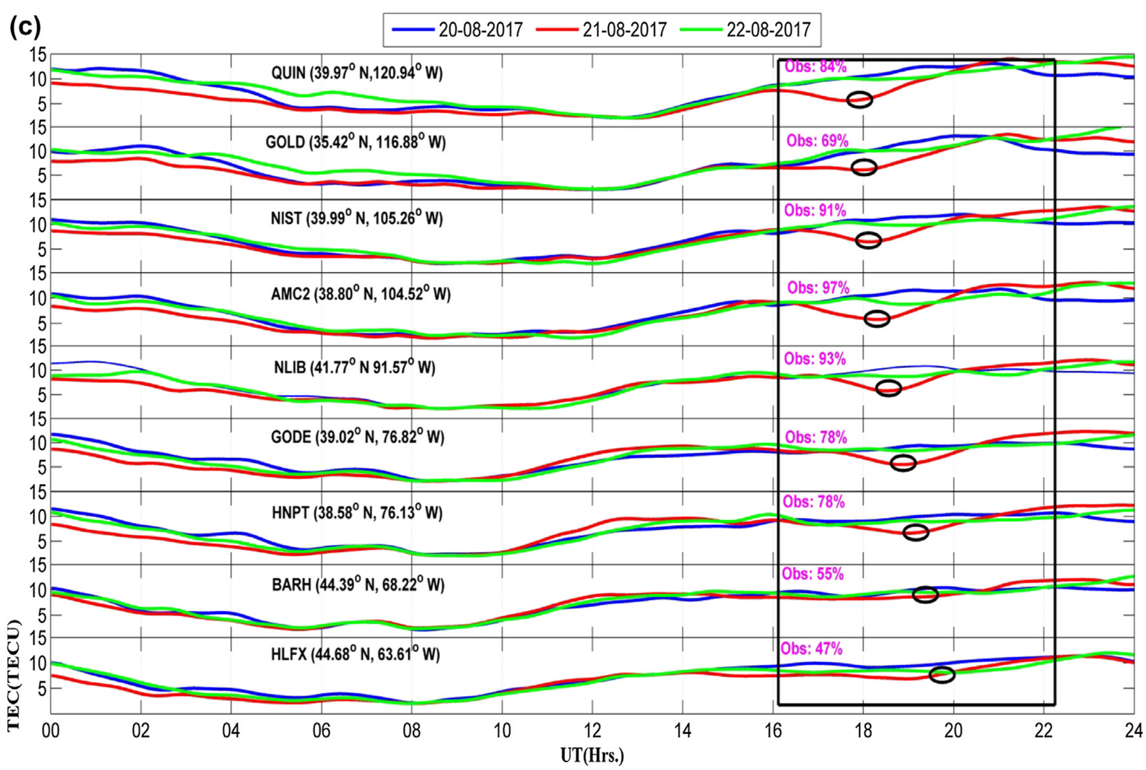

Fig. 7c. The same as Fig. 7a but at ~40° on 21 August 2017.

Zhang et al., 2017; Coster et al., 2017; Nayak and Yigit, 2017; Cherniak and Zekharenkova, 2018) in the USA, where a good number of GPS-based TEC measurements are available.

With regard to the generation mechanism of GWs during eclipse epochs, at the outset, Chimonas and Hines (1970) propose that a solar eclipse can act as a potential source of internal GWs in the ionosphere, which followed the observational evidence of Davis and da Rosa (1970). Research findings of both Chimonas and Hines (1970) and Davis and da Rosa (1970) reported wave-like features in columnar electron content data. Apart from the above, modeling studies have been carried out to predict eclipse-generated GWs in the ionosphere. For example, Fritts and Luo (1993) envisioned that the reduced ozone heating during a solar eclipse generates waves with dominant periods and characteristics in the horizontal and vertical scales of 5000–10,000 km and 200 km, respectively, which can, further, propagate into the upper atmosphere and thermosphere. Müller-Wodarg et al. (1998) modeled in situ eclipse-generated effects in the thermosphere-ionosphere system using the coupled thermosphere/ionosphere plasmasphere model, and their results showed that fluctuations in electron densities propagate as waves, with decreasing amplitudes away (outward) from the path of totality. Similar to the above findings, in the present study, we observed wave-like features of TEC that diminish away from the eclipse path (bow-wave-like signature). Only a few studies have reported on GWs in TEC data triggered by eclipse-associated effects. Jakowski et al. (2008) were the first to report on ionospheric response over Europe for an annual solar eclipse that occurred on 03 October 2005. No wave activity was observed in TEC, but ionosonde and Doppler measurements showed clear-cut wave activity. A study conducted by Kumar et al. (2016) at the equatorial ionization anomaly (EIA) region, i.e., Allahabad (Lat. 25.4° N, Lon. 81.9° E, dip 38.6° N), using GPS-TEC data during a total solar eclipse revealed the presence of GWs with periodicities of approximately 20–45 and 70–90 min at the ionospheric altitudes. As the Kumar et al. (2016) study was restricted to a single station, it was impossible to expect a bow-wave-like response at the ionospheric altitudes. Nevertheless, outstanding results were reported by the Liu et al. (2011) research regarding bow-waves in TEC data in response to a solar eclipse that occurred on 22 July 2009 over the East Asian region, albeit the periodicities were found to be 3–5 min only. Very recently, Verhulst and Stankov (2018) reported a bow-wave-like signature in plasma drift over Europe in response to the 21 August 2017 solar eclipse. It is worth mentioning here that the Verhulst and Stankov (2018) research presented observations from the fringe of the eclipse, whereas our research presented data from the center of the path of totality, but, interestingly, that wave-like nature could still be observed in both these studies.

Concerning our research, we applied a fast Fourier transform (FFT) analysis on TEC data recorded at various individual locations during the eclipse day (not shown here), and we found that periodicities of approximately 55–65 min could be seen, attributed to the GWs. The observed GWs show great similitude with the earliest researchers' results presented on this eclipse (see, for example, Nayak and Yigit, 2017). The research findings of Nayak and Yigit, 2017 showed dominant GWs generated during this solar eclipse event, observed between ~20 and ~90 min, but Nayak and Yigit (2017) used the Hilbert-Huang Transform (HHT, Huang et al., 1998) technique to present various waves associated with this solar eclipse event.

It is highly, therefore, worth mentioning here that solar eclipses do provide an excellent opportunity to better delineate the process of creation and dissipation of GWs in the ionosphere. Although the generation of GWs during a solar eclipse event could be attributed to sharp temporally well-defined changes of solar flux, the dissipation of GWs in the ionosphere depends on thermal conduction and ion drag and others (Yiğit et al., 2009). During an eclipse epoch, the usual processes of production and ionospheric loss are disturbed locally for a brief period (Van Zandt et al., 1960; West et al., 2008). However, during the de-obscuration time, the increasing solar flux starts ionization processes and warms the atmosphere again to daytime level. Such changes in the ionization cause variation in the reflection heights, decrease/increase in electron concentration at all ionospheric heights, decrease/increase in the total electron content, increase/fall in the layer height, and such features are also reported in the present study.

As the presence of GWs is evident during this eclipse event (Nayak and Yigit, 2017; Zhang et al., 2017), a few questions will immediately pop-up in mind that in what way the generated GWs can impact electric fields in the overlying ionosphere? In this context, various earlier studies have shown theoretically and experimentally that GW-associated neutral wind could generate a polarization electric field in the ionospheric E-layer owing to differential collisions between neutral-ion and neutral-electron pairs in the E-layer (Gelinas et al., 2002; Chu et al., 2010a, Chu 2010b). Particularly, Chu et al. (2010a), (2010b) showed schematically how a polarization electric field could generate plasma structure by a gravity-wave-induced neutral wind. According to Chu et al. (2010a), (2010b), a wave-induced polarization electric field gives rise to the drift of ions and electrons in the sporadic-E layer (Es-layer) through the $E \times B$ drifts. Regarding the electric field mapping between the E and F regions of the ionosphere, various earlier studies have provided significant evidence on that aspect (for example, Tsunoda and Cosgrove, 2001; Haldoupis et al., 2003; Shalimov and Haldoupis, 2005). Tsunoda and Cosgrove (2001) suggested that there is a large feedback polarization electric field mapped from the E layer and that ultimately maps to the F-region to produce ionospheric irregularities (popularly known as spread F on ionograms). Besides, according to the Haldoupis et al. (2003) model, the eastward polarization electric fields set up inside the unstable sporadic-E plasma patches can map along the magnetic field lines up to the F region. There, they cause rapid upward and northward $E \times B$ plasma transport that creates abrupt F-region uplifts and spreads F irregularities and ionospheric scintillations, and such mechanism is considered to occur at low latitudes according to the Patra et al. (2009) research. However, an inclusive study with multiple instruments having a high sampling rate along the eclipse path is very much essential to understand wave-like signatures in the overlying ionosphere triggered by eclipse-associated effects (Stankov et al., 2017).

5. Conclusion

Ionospheric responses to a total solar eclipse that occurred on 21 August 2017 over the US region are reported using various remote sensing instruments including MHO, digital ionosonde radars, COSMIC RO, and ground-based GPS TEC receivers. The results were observed to be significant, which are summarized as follows:

I. A 30% reduction in the ionospheric F_2-layer electron densities over MHO incoherent scatter radar was noticed on 21 August 2017. This huge reduction over this radar station during an eclipse event is reported after 33 years, and the earlier one that occurred over this location was on 30 May 1984 (Salah et al., 1986).
II. GPS-based TEC data at ~20°, ~30°, and ~40° N latitudes from the west to east longitudes show considerable depressions and wave-like nature in TEC only during the eclipse day. Further, such depressions slowly decrease when viewed away from the eclipse path and show maximum amplitudes at a station where maximum obscuration has occurred, a clear indication of a bow-wave in TEC data.
III. Ionospheric parameters as measured by ionosondes over Boulder (40.4°N, 100°E) and Austin (30.4°N, 94.4°E) show a significant decrease in critical frequencies, while an altitude elevation is seen in virtual heights of the F-layer only during the eclipse day, and such decreases could be associated with wave-like signatures.
IV. The estimated vertical electron density profile from the COSMIC RO technique shows a maximum depletion of 40%.
V. As the presence of GWs is observed during this total solar eclipse period confidently by virtue of the huge availability of ground-based GPS receivers over the US region (Zhang et al., 2017; Nayak and Yigit, 2017), it may be likely that the eclipse-generated waves could be the responsible sources to create wave-like variations in TEC and ionosonde-scaled parameters (virtual heights and critical frequencies).
VI. FFT analysis on TEC data recorded at various ground-based GNSS stations reveals the dominance of GW periods of ~55–65 min, which show great similitude with earliest researchers' results presented on this eclipse (Nayak and Yigit, 2017).

Acknowledgments

The corresponding author, Dr. P. S. Brahmanandam, gratefully acknowledges the Management of SVECW (Autonomous), Bhimavaram, Andhra Pradesh, India, for their logistic support. Dr. G. Uma is very much grateful to the Department of Science and Technology (DST), Government of India, India for providing a Women Scientist Scheme-A (File no.: SR/WOS-A/EA-1015/2015), in the form of a major research project that enabled her to carry-out this work. Geomagnetic indices including Ap and Kp indices were archived from http://wdc.kugi.kyoto-u.ac.jp/cgi-bin/kp-cgi. The COSMIC RO temperature data are archived from the COSMIC Data Analysis and Archive Center (CDAAC). Observations at Millstone Hill are supported by the U.S. National Science Foundation grant AGS-1242204 under Cooperative Agreement with the Massachusetts Institute of Technology.

References

Anthes, R.A., 2011. Exploring Earth's atmosphere with radio occultation: contributions to weather, climate and space weather. Atmos. Meas. Tech. 4, 1077–1103.

Brahmanandam, P.S., Chu, Y.-H., Liu, J., 2010. Observations of equatorial kelvin wave modes in FORMOSAT-3/COSMIC GPS RO temperature profiles. Terr. Atmos. Ocean. Sci. 21 (5), 829–840.

Brahmanandam, P.S., Chu, Y.H., Wu, K.-H., Hsia, H.-P., Su, C.L., Uma, G., 2011. Vertical and longitudinal electron density structures of equatorial E and F regions. Ann. Geophys. 29 (81–89), 2011. https://doi.org/10.5194/angeo-29-81-2011.

Brahmanandam, P.S., Uma, G., Liu, J.Y., Chu, Y.H., Latha Devi, N.S.M. P., Kakinami, Y., 2012. Global S_4 index variations observed using FORMOSAT-3/COSMIC GPS RO technique during a solar minimum year. J. Geophys. Res. 117 (A09322), 2012. https://doi.org/10.1029/2012JA017966.

Brahmanandam, P.S., Chu, Y.H., Su, C.L., Lin, T.H., 2013. Daytime E-region irregularities during the 22 July 2009 solar eclipse over Chung-Li (24.9°N, 121.2°E), a moderate mid-latitude station. Terr. Atmos. Ocean. Sci. 24, 1021–1032. https://doi.org/10.3319/TAO.2013.07.08.01 (AA).

Cheng, K., Huang, Y.N., Chen, S.W., 1992. Ionospheric effects of the solar eclipse of September 23, 1987, around the equatorial anomaly crest region. J. Geophys. Res. 97, 103–111. https://doi.org/10.1029/91JA02409.

Cheng, C.-Z.F., Kuo, Y.-H., Anthes, R.A., Wu, L., 2006. Satellite constellation monitors global and space weather. Eos Trans., AGU 87 (17), 166.

Cherniak, Zekharenkova, 2018. Ionospheric total electron content response to the great American solar eclipse of 21 August 2017. Geophys. Res. Lett. 45, 1199–1208. https://doi.org/10.1002/2017GL075989.

Chimonas, G., 1970. Internal gravity-wave motions induced in the Earth's atmosphere by a solar eclipse. J. Geophys. Res. 75 (28), 5545–5551. https://doi.org/10.1029/JA075i028p05545.

Chimonas, G., Hines, C.O., 1970. Atmospheric gravity waves induced by a solar Eclipse. J. Geophys. Res. 75, 857–875. https://doi.org/10.1029/JA075i004p00875.

Chu, Y.-H., Wu, K.-H., Su, C.-L., 2009. A new aspect of ionosphericEregion electron density morphology. J. Geophys. Res. 114, A12314. https://doi.org/10.1029/2008JA014022.

Chu, Y.H., Brahmanandam, P.S., Wang, C.Y., Su, C.L., 2010a. Co-ordinated observations of sporadic E using Chung-Li 30 MHz radar, ionosonde and FORMOSAT-3/COSMIC satellites. J. Atmos. Sol. Terr. Phys. 73, 883–894. https://doi.org/10.1016/j.jastp.2010.10.004.

Chu, Y.H., Kong-Hong, Wu., Ching-Lun, Su, 2010b. Reply to comment by Jiuhou Lei et al. on "A new aspect of ionospheric *E* region electron density morphology". J. Geophys. Res. 115, A07314. https://doi.org/10.1029/2010JA015334.

Coster, A.J., Goncharenko, L., Zhang, S.-R., Erickson, P.J., Rideout, W., Vierinen, J., 2017. GNSS observations of ionospheric variations during the 21 August 2017 solar eclipse. Geophys. Res. Lett. 44, 12041–12048. https://doi.org/10.1002/2017GL075774.

Davis, M.J., da Rosa, A.V., 1969. Traveling ionospheric disturbances originating in the auroral oval during polar substorms. J. Geophys. Res. 74 (24), 5721–5735. https://doi.org/10.1029/JA074i024p05721.

Evans, J.V., 1965a. On the behavior of foF2 during solar eclipses. J. Geophys. Res. 70, 733–738. https://doi.org/10.1029/JZ070i003p00733.

Evans, J.V., 1965b. An F region eclipse. J. Geophys. Res. 70, 131–142. https://doi.org/10.1029/JZ070i001p00131.

Fritts, D.C., Luo, Z., 1993. Gravity wave forcing in the middle atmosphere due to reduced ozone heating during a solar eclipse. J. Geophys. Res. 98, 3011–3021. https://doi.org/10.1029/92JD02391.

Gelinas, L.J., Kelley, M.C., Larsen, M.F., 2002. Large-scale E-region electric field structure due to gravity wave winds. J. Atmos. Sol. Terr. Phys. 64, 1465–1469. https://doi.org/10.1016/S1364-6826(02)00110-4.

Gerasopoulos, E., Zerefos, C.S., Tsagouri, I., Founda, D., Amiridis, V., Bais, A.F., Belehaki, A., Christou, N., Economou, G., Kanakidou, M., Karamanos, A., Petrakis, M., Zanis, P., 2008. The total solar eclipse of March 2006: overview. Atmos. Chem. Phys. 8, 5205–5220. https://doi.org/10.5194/acp-8-5205-2008.

Haldoupis, C., Kelley, M.C., Hussey, G.C., Shalimov, S., 2003. Role of unstable sporadic-E layers in the generation of mid-latitude spread F. J. Geophys. Res. 108 (A12), 1446. https://doi.org/10.1029/2003JA009956.

Holt, J.M., Zhang, S.-R., Buonsanto, M.J., 2002. Regional and local ionospheric models based on Millstone Hill incoherent scatter radar data. Geophys. Res. Lett. 29 (8), 1207. https://doi.org/10.1029/2002GL014678.

Huang et al., 1998. The empirical mode decomposition and the Hilbert spectrum for nonlinear and non-stationary time series analysis. Proc. R. Soc. London. 454, 903–995.

Huba, J.D., Drob, D., 2017. SAMI3 prediction of the impact of the 21 August 2017 total solar eclipse on the ionosphere/plasmasphere system. Geophys. Res. Lett. 44, 5928–5935. https://doi.org/10.1002/2017GL073549.

Jakowski et al., 2008. Ionospheric behavior over Europe during the solar eclipse of 3 October 2005. J. Atmosph. Solar Terrest. Phys. 70 (6), 836–853. https://doi.org/10.1016/j.jastp.2007.02.016.

Kumar, K.V., Maurya, A.K., Kumar, S., Singh, R., 2016. 22 July 2009 total solar eclipse induced gravity waves in ionosphere as inferred from GPS observations over EIA. Adv. Space Res. 58, 1755–1762.

Kursinski, E.R., Hajj, G.A., Hardy, K.R., Schofield, J.T., Linfield, R., 1997. Observing Earth's atmosphere with radio occultation measurements. J. Geophys. Res. 102, 23429–23465.

Liu, J.Y., Sun, Y.Y., Kakinami, Y., Chen, C.H., Lin, C.H., Tsai, H.F., 2011. Bow and stern waves triggered by the Moon's shadow boat. Geophys. Res. Lett. 38, L17109. https://doi.org/10.1029/2011GL048805.

Mitra, 1952. The D-layer of the ionosphere. J. Geophys. Res. 56 (3), 373–402. https://doi.org/10.1029/JZ056i003p00373.

Müller-Wodarg, I.C.F., Aylward, A.D., Lockwood, M., 1998. Effects of a mid-latitude solar eclipse on the thermosphere and ionosphere—a modelling study. Geophys. Res. Lett. 25, 3787–3790. https://doi.org/10.1029/1998GL900045.

Nayak, C., Yigit, E., 2017. GPS-TEC observation of gravity waves generated in the ionosphere during 21 August 2017 total solar eclipse. J. Geophys. Res. 122, 725–738. https://doi.org/10.1002/2017JA024845.

Patra, A.K., Venkateswara Rao, N., Phanikumar, D.V., Chandra, H., Das, U., Sinha, H.S.S., Pant, T.K., Sripathi, S., 2009. A study on the low-latitude daytime E region plasma irregularities using coordinated VHF radar, rocket-borne, and ionosonde observations. J. Geophys. Res. 114, A11301. https://doi.org/10.1029/2009JA014501.

Pitout, F., P. Blelly, and Marchaudon A., 2008. EISCAT observations and TRANSCAR simulation of the solar eclipse of August 1, 2008. Eos. Trans. AGU, 89(53), Fall Meet. Suppl., Abstract SA33B–1639.

Potula, B.S., Chu, Y.-H., Uma, G., Hsia, H.-P., Wu, K.-H., 2011. A global comparative study on the ionospheric measurements between COSMIC radio occultation technique and IRI model. J. Geophys. Res. 116 (A02310), 2011. https://doi.org/10.1029/2010JA015814.

Rishbeth, H., Garriott, O.K., 1969. Introduction to ionospheric physics, 331.

Salah, J.E., Oliver, W.L., Foster, J.C., Holt, J.M., Emery, B.A., 1986. Observations of the May 30, 1984, annular solar eclipse at Millstone Hill. J. Geophys. Res. 91, 1651–1660. https://doi.org/10.1029/JA091iA02p01651.

Shalimov, S., Haldoupis, C., 2005. E-region wind-driven electrical coupling of patchy sporadic-E and spread-F at mid latitude. Ann. Geophys. 23, 2095–2105.

Stankov et al., 2017. Multi-instrument observations of the solar eclipse on 20 March 2015 and its effects on the ionosphere over Belgium and Europe. J. Space Weather Space Clim. 7, A19. https://doi.org/10.1051/swsc/2017017.

Tsunoda, R.T., Cosgrove, R.B., 2001. Coupled electrodynamics in the nighttime mid-latitude ionosphere. Geophys. Res. Lett. 28, 4171–4174. https://doi.org/10.1029/2001GL013245.

Uma, G., Brahmanandam, P.S., Chu, Y.H., 2016. A long-term study on the deletion criterion of questionable electron density profiles caused by ionospheric irregularities - COSMIC radio occultation technique. Adv. Space Res. 57 (2), 2452–2463. https://doi.org/10.1016/j.asr.2016.03.034.

Uma, G., Brahmanandam, P.S., Tulasi Ram, S., Wu, K.-H., Chu, Y.H., 2019. A complete solar cycle (2006–2016) studies of scale heights derived using COSMIC radio occultation retrieved electron density profiles. J. Atmos. Sol. Terr. Phys. 182, 101–118. https://doi.org/10.1016/j.jastp.2018.11010.

Van Zandt, T.E., Norton, R.E., Stonehocker, G.H., 1960. Photochemical rates in the equatorial F2 region from the 1958 eclipse. J. Geophys. Res. 65, 2003–2009. https://doi.org/10.1029/JZ065i007p02003.

Verhulst, T.G.W., Sapundjiev, Danislav, Stankov, Stanimir M., 2016. High- resolution ionospheric observations and modeling over Belgium during the solar eclipse of 20 March 2015 including first results of ionospheric tilt and plasma drift measurements. Adv. Space Res. 57, 2407–2419. https://doi.org/10.1016/j.asr.2016.03.009.

Verhulst, T.G.W., Stankov, Stanimir M., 2018. Ionospheric wave signature of the American solar eclipse on 21 August 2017 in Europe. Adv. Space Res. 61, 2245–2251. https://doi.org/10.1016/j.asr.2018.02.007.

West, K.H., Goldsmith, G., Campbell, D., Zandstra, S., 2008. Effects of the 16 February 1980 solar eclipse on the composition of the low-latitude ionosphere as seen by Atmosphere Explorer E. J. Geophys. Res. 113, A12308. https://doi.org/10.1029/2007JA012997.

Wu, Kang-Hung Wu, Ching-Lun, Su, Chu, Yen-Hsyang, 2015. Improvement of GPS radio occultation retrieval error of E region electron density: COSMIC measurement and IRI model simulation. J. Geophys., Res.-Space Phys. 120, 2299–2315. https://doi.org/10.1002/2014JA020622.

Yiğit, E., Medvedev, A.S., Aylward, A.D., Hartogh, P., Harris, M.J., 2009. Modeling the effects of gravity wave momentum deposition on the general circulation above the turbopause. J. Geophys. Res. 114, D07101. https://doi.org/10.1029/2008JD011132.

Zhang, S.-R., Erickson, P.J., Goncharenko, L.P., Coster, A.J., Frissell, N. A., 2017. Monitoring the geospace response to the Great American Solar Eclipse on 21 August 2017. Earth Planet. Phys. 1, 72–76, http://doi.org/10.26464/epp2017011.